Polarization dynamics of a $J=\frac{1}{2}\leftrightarrow J=\frac{1}{2}$ anisotropic laser

R. J. Ballagh and N. J. Mulgan
Physics Department, University of Otago, Dunedin, New Zealand
(Received 16 March 1995; revised manuscript received 9 August 1995)

A theoretical treatment is given of the dynamical and steady-state behavior of an anisotropic laser. The model is based on a homogeneously broadened, pumped $J=\frac{1}{2}\leftrightarrow J=\frac{1}{2}$ atomic transition, and is solved to all orders of the electric field, in contrast to previous studies of anisotropic lasers. A survey of the system behavior is presented, and complementary analytic descriptions developed to describe the small- and large-field evolutions are given. The small-field polarization behavior is shown to be oscillatory in general, and dominated by the properties of the cavity. The large-field description allows the polarization stability of the final output states to be analyzed, and shows that stable steady states in this regime must be linearly polarized along either one or the other of the two anisotropy axes. The possible range of cavity lengths which allows bistable output between these two polarizations is characterized analytically, and a regime identified where the polarization undergoes sustained oscillation.

PACS number(s): 42.60.Gd, 42.50.Ne

I. INTRODUCTION

Laser dynamics is a subject of enduring interest. Most of the attention has been directed to the so-called scalar case, where an internal element such as a Brewster window enforces a single linear polarization on the laser field. Within this context, a rich variety of phenomena has been investigated, including spontaneous pulsation [1], nonlinear dynamics and chaos (e.g., see [2] and references therein), and more recently transverse spatial effects, e.g., [3]. However, the role that the field polarization can play in laser behavior has been known from the earliest experimental investigations of lasers (e.g., [4,5]) and important fundamental theoretical papers [6–8] followed soon after, to build the framework for the treatment of anisotropic lasers. Interest continues to the present day: recent theoretical work has distinguished the fundamental topology of the vectorial laser from the scalar case [9], and shown the influence that different polarization geometries can exert on the dynamical behavior [10].

In this paper, we consider a particular model of the anisotropic laser, in which an isotropic medium couples orthogonal polarizations, and the cavity has a small asymmetry (in phase and absorption) between orthogonal linear polarized modes. Models of this general type, but using a perturbative approximation to the atomic response function, were described in the papers of van Haeringen [6,11] and Tomlinson and Fork [8,12]. Le Floch and co-workers have made an intensive experimental and theoretical study of many aspects of anisotropic lasers [13–16], and have pointed out the advantage that a vectorial laser, with its two distinct modes and easily manipulated coupling, may have over a scalar laser in the study of dynamics. The theoretical part of their work, which has included descriptions of phase transition analogies [14], nonlinear dynamics [15], and vectorial bistability and instabilities [17,18,16] has been based on the equations of the earlier formulations (e.g., see Eqs. (1)–(3), Ref. [12]). Grossmann and Yao [19] have also used similar equations to analyze the output states and stability of a laser with a cavity phase anisotropy.

All of these works have used a perturbative (third-order) atomic response function. However, previous work in different areas of nonlinear optics has shown that a full nonperturbative treatment for the response function of a Zeeman degenerate transition can give rise to surprisingly distinctive phenomena. For example, in passive optical bistability, the stable output states of a $J=\frac{1}{2}\leftrightarrow J=\frac{1}{2}$ transition driven by linearly polarized light are circularly polarized [20], while for a $J_\ell=1\leftrightarrow J_u=0$ transition the output polarization is identical to the input [21,22]. In nonlinear beam propagation, a $J=\frac{1}{2}\leftrightarrow J=\frac{1}{2}$ transition may cause an elliptically polarized Gaussian beam to develop into concentric rings of alternate circular polarization [23–25], while a $J_\ell=1\leftrightarrow J_u=0$ transition preserves the initial polarization across the spatial profile [26]. The effect that such nonperturbative response functions might have on laser dynamics is thus not easily predicted. Recently a saturating response has been used by Eschmann and Gardiner [27] in the somewhat different context of modeling the stability properties of two adjacent whispering gallery lasers.

In the present paper we wish to revisit the treatment of anisotropic lasers, to explore the effect that a fully nonperturbative treatment of a homogeneously broadened $J=\frac{1}{2}\leftrightarrow J=\frac{1}{2}$ transition will have on the laser dynamics. The response function we find for this transition is intrinsically isotropic, but incorporates absorptive and dispersive saturation and mediates a competitive nonlinear coupling between left and right circular polarizations, driven by optical pumping in the lower level. The anisotropy of the laser arises entirely from the cavity, which we assume to be a ring supporting two orthogonal linearly polarized modes with slightly differing frequencies and decay rates. The basic equations for the two modes are derived in Sec. II by employing an adiabiatic elimination of the atomic medium. A survey of the type of system behavior this model laser can exhibit over a wide range of parameter space is given in Sec. III, and we then develop two complementary approximate

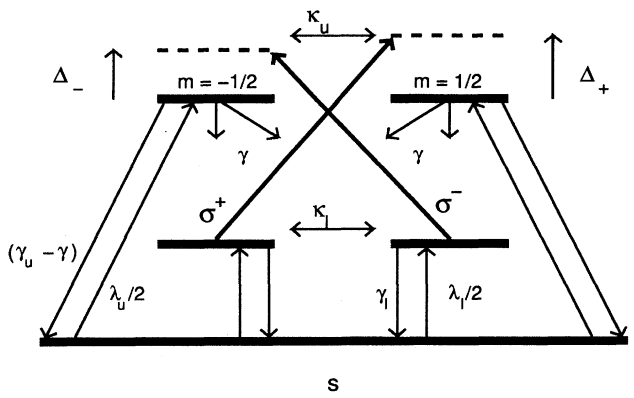

FIG. 1. The atomic system, consisting of a $J=\frac{1}{2}\leftrightarrow J=\frac{1}{2}$ transition plus a reservoir state (s).

descriptions to explain the dynamical behavior. The first of these (Sec. IV A) applies during the initial period while the laser intensity is small, and describes the evolution of the polarization ellipse. The second (Secs. IV B and V) describes the rate of precession of the polarization ellipse, once the field has become large, and allows us to identify quantitatively the possible output polarizations and their stability. We find and characterize one parameter regime where the output polarization undergoes oscillation, and we also characterize the parameter regime where a previously noted polarization flipping [6] and bistability [17] of the two linear polarizations can occur.

II. BACKGROUND

Our model is formulated under the assumption that the atomic medium can be adiabatically eliminated from the full system equations, allowing the steady-state quantum-mechanical expectation value of the atomic dipole to be used in the electric field equations. In this section, we begin by presenting our atomic model and its steady-state solutions, and then proceed to obtain our basic laser equations by using appropriate vectorial boundary conditions in Maxwell's equations. Although adiabatic elimination is a common technique in treatments of laser dynamics (e.g., see Refs. [2,28]), some discussion of its implications is required in the present case, since our atomic model is rather more complex than the familiar two-state model. For convenience, we give this discussion at the end of this section once all the properties and parameters of the full system have been introduced.

A. Atomic model

The response function of a homogeneously broadened $J=\frac{1}{2}\leftrightarrow J=\frac{1}{2}$ transition with isotropic relaxation has previously been solved for an isolated system (i.e., without pumping) by Hamilton *et al.* [20,29] (and see [23]). Their solution gives the circular components of the macroscopic polarization expressed as closed functions of the σ^+ and σ^- electric field amplitudes and detunings. In this paper we modify the $J=\frac{1}{2}\leftrightarrow J=\frac{1}{2}$ model to introduce gain to the system by incorporating pumping from a fifth (reservoir) state, as shown in Fig. 1. The upper (u) and lower (l) levels are separated by energy $\hbar\omega_{ul}$ and are isotropically pumped from the reservoir state at rates λ_u and λ_ℓ, respectively, while decaying isotropically at rates γ_u and γ_ℓ. Population transfers spontaneously from the upper to lower level at rate γ and is transferred collisionally between the lower states at rate κ_ℓ and between the upper states at rate κ_u. The atoms interact with a coherent classical electric field which propagates in the z direction and can be written

$$\mathbf{E}(\mathbf{r},t)=E_{\rm sat}\mathscr{E}(\mathbf{r},t)e^{i(kz-\omega t)}+\text{c.c.}, \tag{1}$$

where ω is a conveniently chosen center frequency which we describe further at the end of Sec. II B. The saturation electric field $E_{\rm sat}$ is

$$E_{\rm sat}=\frac{\hbar}{d_{u\ell}}\sqrt{\frac{6\Gamma\gamma}{\mu}}, \tag{2}$$

where $d_{u\ell}$ is the reduced matrix element for the transition and Γ is the relaxation rate of the electric dipole. The quantity μ (defined below) is a measure of the change in saturation due to the pumping from, and decay to, the reservoir state. Writing the vector amplitude $\mathscr{E}(\mathbf{r},t)$ as

$$\mathscr{E}(\mathbf{r},t)=\mathscr{E}_+(\mathbf{r},t)\hat{\mathbf{e}}^*_{-1}+\mathscr{E}_-(\mathbf{r},t)\hat{\mathbf{e}}^*_{+1}, \tag{3}$$

where $\hat{\mathbf{e}}^*_{\pm 1}$ are standard spherical basis vectors (e.g., see p. 28 of [30]), then $\mathscr{E}_+$ and $\mathscr{E}_-$ represent the slowly varying complex amplitude of the σ^+ (left circular polarized [31]) and σ^- (right circular polarized) components, respectively.

We write [20] the macroscopic polarization in terms of irreducible tensor components [32] of the atomic density matrix

$$\mathbf{P}=\frac{d_{u\ell}N}{\sqrt{3}V}\sum_q \hat{\mathbf{e}}^*_q\{(-1)^q\rho^1_{-q}(\ell u;\mathbf{r},t)+[\rho^1_q(\ell u;\mathbf{r},t)]^*\}, \tag{4}$$

where N/V is the atomic density, and find steady-state solutions for $\rho^1_{-q}(\ell u;\mathbf{r},t)$ by solving the density matrix master equation presented in Appendix A. Writing

$$\mathbf{P}=\vec{\mathscr{P}}e^{i(kz-\omega t)}+\text{c.c.}, \tag{5}$$

the steady-state positive frequency macroscopic polarization has the form

$$\vec{\mathscr{P}}=-i\frac{N}{V}d_{u\ell}\sqrt{\frac{2\gamma}{3\Gamma}}n_0[\eta_+\mathscr{E}_+\hat{\mathbf{e}}^*_{-1}+\eta_-\mathscr{E}_-\hat{\mathbf{e}}^*_{+1}], \tag{6}$$

where the zero electric field inversion n_0 is given by

$$n_0=\frac{[\lambda_u(\gamma_\ell-\gamma)-\lambda_\ell\gamma_u]}{[\gamma_\ell\gamma_u+\lambda_u(\gamma_\ell+\gamma)+\lambda_\ell\gamma_u]}, \tag{7}$$

and the circular response functions $\eta_\pm$ are

$$\eta_\pm=\tilde{\eta}_\pm\frac{1+i\Delta_\pm}{1+\Delta_\pm^2}, \tag{8}$$

with

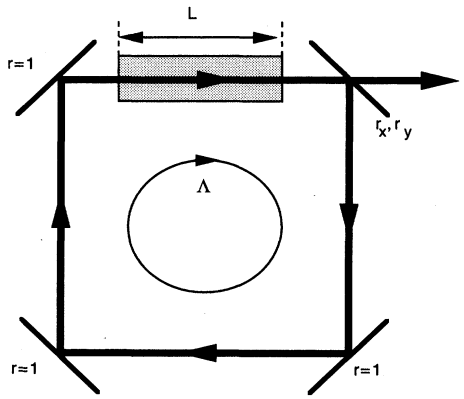

FIG. 2. The anisotropic ring laser. The field is constrained to propagate in one direction only and the output mirror has different (and complex) reflectivities for x and y polarizations. The other mirrors are perfect reflectors.

$$\tilde{\eta}_{\pm}=\frac{1+4\beta I_{\mp}}{1+(2\beta+4)(I_{+}+I_{-})+32\beta I_{+}I_{-}}. \tag{9}$$

The generalized intensities, defined as

$$I_{\pm}\equiv\frac{|\mathscr{E}_{\pm}|^2}{1+\Delta_{\pm}^2}, \tag{10}$$

include the effect of the detunings $\Delta_{\pm}$ of the $\sigma^{\pm}$ fields from resonance,

$$\Delta_{\pm}\equiv\Delta-\frac{1}{\Gamma}\frac{\partial}{\partial t}(\arg(\mathscr{E}_{\pm})), \tag{11}$$

where we have defined

$$\Delta=\frac{\omega-\omega_{u\ell}}{\Gamma}. \tag{12}$$

We note that Eq. (11) accommodates any frequency pulling that might occur. The response functions $\eta_{\pm}$ in Eq. (8) have the same form as the expression obtained by Hamilton *et al.* [29], but the parameter β now incorporates the effect of all the transfer rates,

$$\beta=\beta_u/\mu, \tag{13}$$

with

$$\beta_u=\frac{\gamma}{(\gamma_u+2\kappa_u)(\gamma_\ell+2\kappa_\ell)}(\gamma_u+2\kappa_u+\gamma_\ell+2\kappa_\ell-\gamma/3), \tag{14}$$

and

$$\mu=\frac{\gamma[2(\lambda_u+\lambda_\ell)+\gamma_u+\gamma_\ell-\gamma]}{2[\gamma_\ell\gamma_u+\lambda_u(\gamma_\ell+\gamma)+\lambda_\ell\gamma_u]}. \tag{15}$$

B. Anisotropic ring cavity

In our ring laser (see Fig. 2) we will assume that the electric field is plane wave, constrained to travel in one direction only, and is polarized in the plane perpendicular to that direction. In the slowly varying envelope approximation (SVEA), and with adiabatic elimination of the atoms, Maxwell's equations become

$$\frac{\partial\mathscr{E}}{\partial t}+c\frac{\partial\mathscr{E}}{\partial z}=\frac{i\omega}{2\epsilon_0}\vec{\mathscr{P}}, \tag{16}$$

where $\vec{\mathscr{P}}$ is given by Eq. (6). The cavity, which has round trip length Λ, enters the problem through the boundary conditions imposed on Eq. (16): after exiting the medium the field reflects off the output mirror and then propagates through empty space a distance $\Lambda-L$ before reentering the medium (the other mirrors serve only to redirect the beam). We shall assume the cavity has linear anisotropy, with amplitude reflection coefficients r_x and r_y and empty cavity resonant frequencies ω_x and ω_y, respectively, for x and y polarized fields. In an empty cavity, a round trip phase difference of 2θ develops between x and y polarizations with θ given by

$$\theta=\frac{\Lambda}{c}\frac{\omega_y-\omega_x}{2}. \tag{17}$$

We remark that a choice of circular anisotropy for the cavity leads to dynamics that are essentially those of the well known two-state laser model, and will not be pursued further here. The range of dynamic behavior that we shall see later in this paper results from the coupling between the modes of the cavity which are linear polarized, and the natural modes of the medium, which are circular.

In Appendix B we derive the following boundary conditions for the slowly varying $\sigma^{\pm}$ amplitudes,

$$\begin{pmatrix}\mathscr{E}_{+}(0,t)\\ \mathscr{E}_{-}(0,t)\end{pmatrix}=R_{\rm circ}\begin{pmatrix}\mathscr{E}_{+}\left(L,t-\frac{\Lambda-L}{c}\right)\\ \mathscr{E}_{-}\left(L,t-\frac{\Lambda-L}{c}\right)\end{pmatrix}, \tag{18}$$

where $R_{\rm circ}$ is a 2×2 matrix given by Eq. (B19) and depending only on the cavity parameters r_x, r_y and θ. We note that in deriving Eq. (18) we have chosen the slowly varying frequency ω to be $(\omega_x+\omega_y)/2$.

C. Field equations

The boundary condition, Eq. (18), can be made isochronous and periodic in z by applying a vectorial generalization of the transformation of Lugiato [33]:

$$\begin{pmatrix}\mathscr{E}_{+}(z,t)\\ \mathscr{E}_{-}(z,t)\end{pmatrix}=\exp[-(z/L)\ \ln R_{\rm circ}]\begin{pmatrix}\mathscr{E}'_{+}(z,t')\\ \mathscr{E}'_{-}(z,t')\end{pmatrix}, \tag{19}$$

where $\ln R_{\rm circ}$ is the matrix logarithm of $R_{\rm circ}$ and

$$t'=t+\frac{\Lambda-L}{c}\frac{z}{L}. \tag{20}$$

Since we expect the gain per passage through the medium to be small, we make a uniform field approximation [34]:

$$\mathscr{E}'_{\pm}(z,t')\approx\mathscr{E}'_{\pm}(0,t')\equiv\mathscr{E}'_{+}(t'), \tag{21}$$

which allows for a spatial exponential growth of the field $\mathscr{E}$ in the medium, to balance the loss at the mirrors. Now substituting for $\mathscr{E}$ in the Maxwell-Bloch equation, Eq. (16), we obtain

$$\left[\frac{d}{dt'}-\frac{c}{\Lambda}\ln R_{\rm circ}\right]\begin{pmatrix}\mathscr{E}'_{+}\\ \mathscr{E}'_{-}\end{pmatrix}=\frac{g_0 L}{2}\frac{c}{\Lambda}\begin{pmatrix}\eta_{+} & 0\\ 0 & \eta_{-}\end{pmatrix}\begin{pmatrix}\mathscr{E}'_{+}\\ \mathscr{E}'_{-}\end{pmatrix}, \tag{22}$$

where we have substituted for $\mathscr{P}$ from Eq. (6) and

$$g_0=\frac{\pi n_0 N\gamma c^2}{\Gamma\omega^2 V} \tag{23}$$

is the small-field gain.

Although it is possible to proceed in terms of either x and y polarized components of the fields (the natural basis for the cavity) or σ^+ and σ^- fields (natural for the medium), the complexity of the response functions in an $\hat{\mathbf{e}}_x,\hat{\mathbf{e}}_y$ basis makes the spherical basis the better choice. Setting

$$\mathscr{E}'_{\pm}(t')=\begin{pmatrix}A_{+}(t')e^{-i\phi_{+}(t')}\\ A_{-}(t')e^{-i\phi_{-}(t')}\end{pmatrix}, \tag{24}$$

where $A_{\pm}$ and $\phi_{\pm}$ are real and

$$\delta(t')=\phi_{+}(t')-\phi_{-}(t'), \tag{25}$$

and making the scale change $\kappa t'=\tau$, where

$$\kappa=\frac{c|\ln\sqrt{r_x r_y}|}{\Lambda} \tag{26}$$

is the generalized form of the cavity decay rate of scalar laser theory (Chap. 7 of Ref. [34]), we obtain the fundamental equations of our laser model by taking the real and imaginary parts of Eq. (22), to give

$$\frac{dA_{\pm}}{d\tau}=-\left(1-\frac{C\tilde{\eta}_{\pm}}{1+\Delta_{\pm}^2}\right)A_{\pm}(\tau)+(-\varepsilon\cos\delta\pm\omega_b\sin\delta)A_{\mp}(\tau) \tag{27}$$

and

$$\frac{d\phi_{\pm}}{d\tau}=-\frac{C\Delta_{\pm}\tilde{\eta}_{\pm}}{1+\Delta_{\pm}^2}+(\omega_b\cos\delta\pm\varepsilon\sin\delta)\frac{A_{\mp}(\tau)}{A_{\pm}(\tau)}. \tag{28}$$

In these equations we have introduced the following parameters:

$$C=\frac{g_0 L}{2|\ln\sqrt{r_x r_y}|}, \tag{29}$$

which is the cooperativity (e.g, see Chap. 7 of Ref. [34]), and

$$\varepsilon=\frac{\ln\sqrt{r_y/r_x}}{\ln\sqrt{r_x r_y}}, \tag{30}$$

$$\omega_b=\frac{\theta}{|\ln\sqrt{r_x r_y}|}, \tag{31}$$

where ε (which is positive when $r_x>r_y$) is a measure of the cavity absorption anisotropy and ω_b (half the frequency separation of the empty cavity x and y polarized modes in units of κ) is a measure of the "phase anisotropy." In terms of these quantities, the empty cavity resonant frequencies are at $\omega-\kappa\omega_b$ (x polarization) and $\omega+\kappa\omega_b$ (y), with corresponding decay rates being $\kappa(1-\varepsilon)$ for x and $\kappa(1+\varepsilon)$ for y. We note that the detunings Δ_+ and Δ_- can be expressed in terms of the new variables as

$$\Delta_{\pm}\equiv\Delta+\frac{\kappa}{\Gamma}\frac{d\phi_{\pm}}{d\tau}, \tag{32}$$

which shows that Eqs. (27) and (28) are implicit equations for $d\phi_+/d\tau$ and $d\phi_-/d\tau$. However, ϕ_+ and ϕ_- only appear on the right-hand side (RHS) of these equations in terms of $\delta\,(=\phi_+-\phi_-)$, which means the laser is not sensitive to the individual phases of σ^+ and σ^-, but only to their phase separation and frequencies. We note that a general elliptical polarization state of the field can be described in terms of δ and the quantity ρ, where

$$\rho=A_{+}/A_{-}. \tag{33}$$

When $\delta=0$, the ratio of y to x axes of the ellipse is $(\rho+1)/(\rho-1)$, and a nonzero δ causes the ellipse to be rotated in the positive direction by an amount $\delta/2$. Furthermore, if $\rho>1$, the polarization is left circular and if $\rho<1$ it is right circular.

Equations (27) and (28) form the basis of the rest of this work, and we can identify in them the separate mechanisms which drive the evolution of the fields. The σ^+ amplitude, for example, suffers loss from the cavity (at rate 1 in our scaled units) and gain from the medium at rate $C\mathrm{Re}(\eta_+)$ [together making up the first term in Eq. (27)]. Correspondingly the phase ϕ_+ is modified by the medium dispersion [the $\Delta_+\eta_+$ term of (Eq. (28)]. In addition, both equations have terms in $\sin\delta$ and $\cos\delta$ which represent the conversion of σ^+ into σ^- by the x and y cavity anisotropies.

For later convenience we present the equation for the phase difference δ [obtained from the difference of the two equations, Eq. (28)]:

$$\frac{d\delta}{d\tau}=-C\left(\frac{\Delta_{+}\tilde{\eta}_{+}}{1+\Delta_{+}^2}-\frac{\Delta_{-}\tilde{\eta}_{-}}{1+\Delta_{-}^2}\right)+\omega_b(1/\rho-\rho)\cos\delta+\varepsilon(1/\rho+\rho)\sin\delta. \tag{34}$$

D. Adiabatic elimination

The basic condition for adiabatic elimination of a group of variables is that their relaxation rates are much larger than those for the variables that remain. Given the large number of rates that occur in the $J=\frac{1}{2}\leftrightarrow J=\frac{1}{2}$ model, it is worthwhile to identify the parameter regime for which the adiabatic elimination can be expected to be valid. In so doing we are guided by the systematic procedure for adiabatic elimination provided by Lugiato *et al.* [28]. We begin by considering the

case where all the atomic relaxation rates are of the same order, and we represent a typical atomic rate by Γ_a. The atomic variables are to be considered the "fast" variables, and the smallness parameter of the adiabatic elimination is then $\epsilon=\kappa/\Gamma_a$. By scaling the time variable for the density matrix equations, Eqs. (A1)–(A8), in terms of $\tau=\kappa t$, and dividing each equation through by Γ_a, it is clear that in the limit $\epsilon\rightarrow 0$ all the constants on the RHS of those equations remain finite, and that the temporal derivatives can be neglected. The atomic parameters that remain in the field evolution equations (27) and (28) are C, $\Delta_\pm$, and β and all remain finite in the limit $\epsilon\rightarrow 0$: the first two parameters are defined analogously to the corresponding quantities in Lugiato *et al.* [28], while β is defined in terms of ratios of atomic transfer rates, and hence is independent of scaling. Similarly, our saturation field Eq. (2) is defined as in Lugiato *et al.* [apart from the quantity μ which is also invariant to scaling; see Eq. (15)] and thus we may conclude, using their argument, that the fluctuations do not diverge as $\epsilon\rightarrow 0$ and our semiclassical equations are valid.We note that the cavity anisotropy parameters ε and ω_b are already defined in units of κ and thus are well behaved in the adiabatic limit.

The key atomic rates are γ and γ_l, and we will assume in all that follows that $\gamma_l>\gamma$ since Eq. (7) shows this is necessary in order that our system has gain. Hence for all cases of interest $\beta_u\lesssim 1$ (since $\gamma_u>\gamma$) and in the most typical case, when $\gamma_u+2\kappa_u\approx\gamma$, we have $\beta_u\approx 1$. Without significant loss of generality we can set $\lambda_\ell=0$ and $\gamma_u=\gamma$, so that the value of μ is controlled by λ_u, such that $\mu\rightarrow 1/2$ when $\lambda_u\ll\gamma$ and $\mu\rightarrow\gamma/\gamma_\ell$ when $\lambda_u\gtrsim\gamma_l$. We see therefore that in the case where all atomic decay rates are to be of the same order, we should have $\beta<10$. Accordingly for most of the results we present in this paper, we set $\beta=4$. However, interesting and qualitatively different dynamics also occur for larger values of β. It is clear that these can only be achieved if $\gamma_\ell\gg\gamma$, but providing that the smallest atomic rate is much larger than κ, Lugiato *et al.* have shown that it is possible to proceed with the adiabatic elimination by dividing the variables into three groups, and eliminating first the variables associated with the largest decay rates (in this case including at least γ_ℓ and Γ), and next the variables with the intermediate decay rates (all other atomic variables).

III. RESULTS

The electric field amplitude and phase equations, Eqs. (27) and (28), are a set of first-order ODE's for the variables A_+, A_-, ϕ_+, and ϕ_-, with implicit coefficients (since $d\phi_\pm/d\tau$ appears in $\eta_\pm$). They are integrated numerically by first using a rootfinder to generate, for given A_+, A_-, and δ, solutions to the implicit equations, Eq. (28), for $d\phi_+/d\tau$ and $d\phi_-/d\tau$. The values of $d\phi_+/d\tau$ and $d\phi_-/d\tau$ are then used in Eq. (27) to provide the derivatives $dA_+/d\tau$ and $dA_-/d\tau$ for an ODE solving routine. Thus we see that, although the system as written in Eqs. (27) and (28) is a set of four equations in four variables, in fact only three variables are needed for the solution. Physically the reason for this is clear: only the relative phase between σ^+ and σ^- is required to specify the polarization.

We have investigated this system extensively for a wide range of parameters consistent with the assumptions of adiabatic elimination, small anisotropy ($\varepsilon\ll 1$, $\omega_b^2\ll 1$), and for a range of initial conditions (A_+, A_-, and δ). We have found that there is an overwhelming probability that the system behavior falls into one of three main catergories, which relate to the possible final output states of the laser: (i) cw and linearly polarized along x; (ii) cw and linearly polarized along y; (iii) oscillatory behavior; and we illustrate these behaviors below in Figs. 3–7. In each figure we have set $\varepsilon>0$ (i.e., the x polarized mode has the lowest loss), but the results given are representative of many different simulations, and their character is insensitive to seed intensity (provided the seed is small) although in some (bistable) cases, critically dependent on the seed polarization.

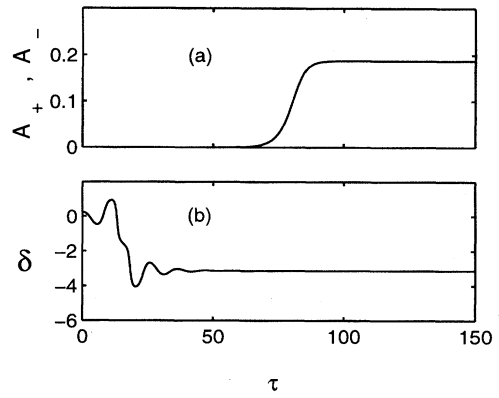

FIG. 3. Laser field evolution for the case $\Delta=0.1$, $\varepsilon=0.07$, $\omega_b=0.3$, $C=1.2$, $\beta=4$, and $\kappa/\Gamma=0.01$. (a) A_+ (solid line) and A_- ($=A_+$ in this case); (b) δ. The initial field is $A_+=A_-=10^{-9}$ and $\delta=\pi/14$.

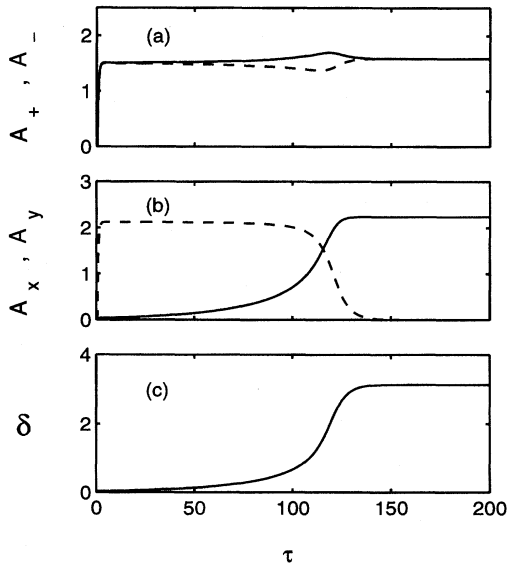

FIG. 4. Laser field evolution for the case $\Delta=0.02$, $\varepsilon=0.05$, $\omega_b=0.2$, $C=20$, $\beta=4$, and $\kappa/\Gamma=0.01$. (a) A_+ (solid line) and A_- (dashed); (b) A_x (solid) and A_y (dashed); (c) δ. The initial field is $A_+=A_-=10^{-6}$ and $\delta=\pi/100$.

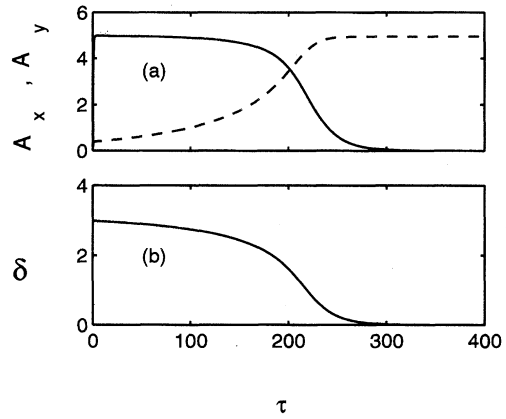

FIG. 5. Laser field evolution for the case $\Delta=-0.25$, $\varepsilon=0.01$, $\omega_b=0.1$, $C=100$, $\beta=4$, and $\kappa/\Gamma=0.01$. (a) A_x (solid) and A_y (dashed); (b) δ. The initial field is $A_+=A_-=10^{-6}$ and $\delta=0.95\pi$.

Figure 3 displays the most common type of behavior, where the system evolves to a cw x polarized output field. We have chosen initial conditions corresponding to linear polarization close to the y axis, and see that while the fields still remain small, an unstable oscillation of the initial phase difference δ leads the polarization to switch to near the x axis ($\delta=\pm\pi$) where it settles down by a damped oscillation. Subsequently the laser intensity grows to its final steady state. A variant of this behavior, in which the y polarized field is "metastable," can also often occur and is shown in Fig. 4, where the intial polarization direction has again been chosen near the y axis. Initially the field amplitudes grow exponentially (while δ does not change significantly), but then level off to a plateau region in which the polarization is almost linear and almost parallel to the y axis. Throughout this time the polarization ellipse slowly rotates, but near $\tau=100$, δ increases rapidly, and the polarization flips to linear x, which is the final stable output state.

The second category of behavior, where the system evolves to a stable y polarized output, is illustrated in Figs. 5

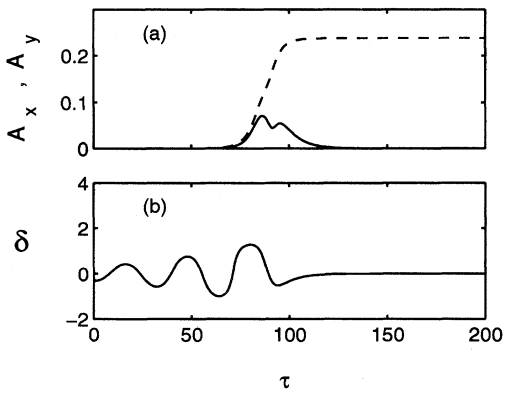

FIG. 6. Laser field evolution for the same parameters as Fig. 5 but with $C=1.3$ and initial field $A_+=A_-=10^{-6}$ and $\delta=-\pi/10$.

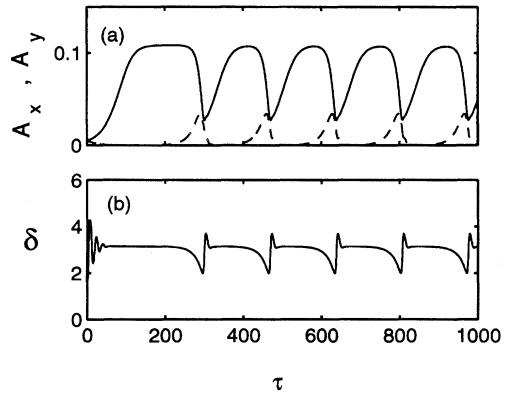

FIG. 7. Laser field evolution for the case $\Delta=-0.63$, $\varepsilon=0.03$, $\omega_b=0.2$, $C=1.4$, $\beta=100$, and $\kappa/\Gamma=0.001$. (a) A_x (solid) and A_y (dashed); (b) δ. The initial field is $A_+=A_-=0.005$ and $\delta=\pi/2$.

and 6. In Fig. 5 the seed field is near the x axis, and the intensity grows rapidly with this polarization, and subsequently the polarization slowly precesses to the y axis. In Fig. 6, where the parameters are the same as in Fig. 5 except C is smaller and the initial polarization direction is near the y axis, the field swings through a sequence of elliptically polarized states before settling to its final value along the y axis. If the detuning Δ is increased, a bistable regime is encountered where steady-state output may be polarized along *either* the x or y axis, depending on the seed field's polarization. Most often, however, only one or other of the orthogonal linear polarizations is stable, as discussed further in Sec. V.

The third main category of system evolution, where the output field undergoes oscillation, is illustrated in Fig. 7. This regime occurs only for a small range of Δ values on one side of resonance. The initial (small-field) behavior ($\tau\lesssim 50$ in this case), which includes a damped oscillation in δ about $\delta=\pi$, is similar to that shown in Fig. 3.

The key parameters in determining the output behavior are ω_b, ε, and Δ, while in most cases the solutions are much less sensitive to β and C [provided of course that C is above threshold; see Eq. (48)]. All of our results are insensitive to the value of Γ provided $\Gamma\gg\kappa$. For Fig. 3, the solution is unchanged if β is increased or decreased by several orders of magnitude, but increasing C allows the solution to have an interim "y-metastable" state for seed fields polarized near y. For all values of β and C, however, simulations with the values of ω_b, ε, and Δ as in Fig. 3 finish in a cw x-polarized steady state. The form of the solution shown in Fig. 4 is unaltered as C increases, and the solution has no sensitivity to β if C is large. However, if C is reduced to near the threshold value, the duration of the metastable polarization increases as β approaches the value 2 (which as shown in Ref. [23] is a special value of β that causes the σ^+ and σ^- response functions to decouple). The solution in Fig. 5 is insensitive to increasing either C or β. For Fig. 6, increasing C shortens the time taken to reach the final y polarization so that the δ oscillations may not have time to occur, but increasing β barely changes the solution. However, decreasing β by two orders of magnitude (while keep-

ing all other parameters in Fig. 6 unchanged) allows the solution to end in an x-polarized state. The oscillatory solutions occur only for a narrow parameter range and display most sensitivity to the values of β and C.

We have been unable to find completely general solutions to analytically verify the dominance of the three classes of behavior discussed above. It is easy to see from Eq. (34), however, that any solution with a constant linear polarization ($A_+=A_-$ and $d\delta/d\tau=0$) must be polarized along either the x or y axis ($\delta=0$ or $\pm\pi$, respectively). On the other hand, steady-state elliptically polarized solutions with constant amplitudes A_+ and A_- cannot be ruled out. We have thus been led to an alternative and approximate analytic treatment in order to understand the types of behavior the system exhibits. A detailed discussion of this treatment is given in the remaining sections of this paper, and we find we are able to quantify the parameter regimes for which the three types of behavior given above may occur.

IV. ANALYTIC DESCRIPTION OF DYNAMICS

The evolution of the laser field can be well described by two complementary analytic approximations. The first, which we shall call the small-field approximation, describes the behavior from initial turn on, until the intensities of the σ^+ and σ^- fields are no longer small. The second, which we shall call the large-field approximation, describes the evolution of the phase difference once the field amplitudes have become sufficiently large. This latter approximation will allow us to predict the stability properties of the output states in the large-field regime and, together with the small-field approximation, allow the origin of the behavior types discussed in Sec. III to be understood.

A. Initial behavior

When the fields are small the response functions simplify to

$$\tilde{\eta}_\pm \approx 1, \tag{35}$$

provided

$$(2\beta+4)I_\pm \ll 1 \quad \text{if} \quad I_\pm \gg I_\mp \tag{36}$$

or

$$8I_\pm \ll 1 \quad \text{if} \quad I_+=I_-. \tag{37}$$

For the cases of small fields polarized along either the x or y axes, then Eq. (28) becomes

$$\frac{d\phi_+}{d\tau} \approx -\frac{C\Delta_+}{1+\Delta_+^2} \pm \omega_b, \tag{38}$$

where the upper sign refers to y polarization, the lower to x polarization, and a similar equation holds for $d\phi_-/d\tau$. If $\kappa/\Gamma \ll 1$ (as it must if the adiabatic elimination is to be valid) and also

$$\frac{\kappa}{\Gamma}\frac{C}{(1+\Delta^2)} \ll 1, \tag{39}$$

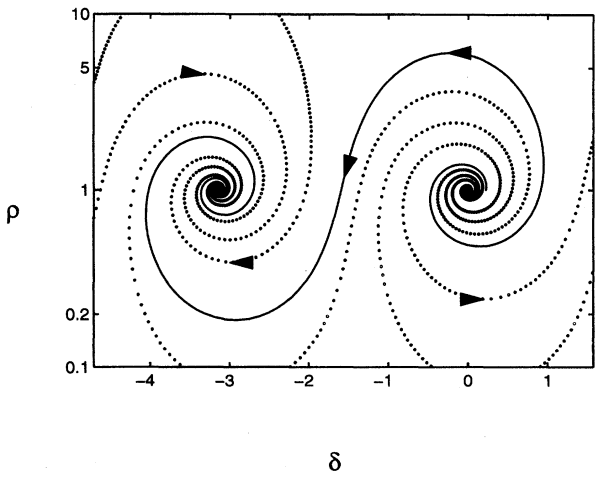

FIG. 8. Example trajectories (dotted lines) in the ρ ($\equiv A_+/A_-$) and δ plane for the small field equations (42) and (43). Parameters are exactly as in Fig. 3, and the trajectory corresponding to Fig. 3 is shown as the solid curve.

then it is clear from Eq. (32) and (38) that

$$1+\Delta_\pm^2 \approx 1+\Delta^2. \tag{40}$$

Strictly, Eq. (40) has been derived only for small fields linearly polarized along x and y, but a similar (although algebraically more tedious) argument can be used to validate Eq. (40) for an arbitrarily polarized small field. We are now able to write an approximate form of the equation for $d\delta/d\tau$. Applying Eq. (35) and Eq. (40) to the equation for $d\delta/d\tau$, we find the first term in Eq. (34) reduces to

$$-\frac{\kappa C}{\Gamma(1+\Delta^2)}\frac{d\delta}{d\tau} \tag{41}$$

which is a negligible correction to the derivative on the left-hand side of the equation, and thus we obtain

$$\frac{d\delta}{d\tau} \approx \left[\left(\frac{1}{\rho}-\rho\right)\omega_b \cos\delta + \left(\frac{1}{\rho}+\rho\right)\varepsilon \sin\delta\right], \tag{42}$$

which is valid for a general polarization in the small-field regime. Similarly, beginning with $\rho=A_+/A_-$ and Eq. (27), and using the same approximations that lead to Eq. (42), we obtain the following equation for $d\rho/d\tau$:

$$\frac{d\rho}{d\tau} = [(\rho^2-1)\varepsilon \cos\delta + (\rho^2+1)\omega_b \sin\delta]. \tag{43}$$

Equations (42) and (43) constitute a closed set of equations [35], which describe the evolution of δ and ρ while the electric field remains small. We interpret these equations physically by noting that in the low-field regime the medium contributes symmetrically to the individual phases and amplitudes, and thus ρ and δ are driven only by the cavity anisotropy. The critical points for the equations (where $d\rho/d\tau=0$ and $d\delta/d\tau=0$) occur at $\rho=1$ and $\delta=0, \pm\pi$, and a linear stability analysis about these points shows that for

small fields, linear y polarization ($\delta=0,\rho=1$) is unstable, while linear x polarization ($\delta=\pm\pi,\rho=1$) is stable. Physically, this could be expected, as A_x experiences less loss at the mirrors than A_y.

In Figs. 8 and 9 we plot as dotted lines in δ-ρ space example trajectories obtained by solving Eqs. (42) and (43) for a variety of seed fields. These trajectories are double spirals that flow outwards from linear polarized y, and eventually flow into linearly polarized x. We also show the actual trajectories (solid lines) corresponding to the full solutions in Figs. 3 and 6, and see that in the former case (Fig. 8) the full solution follows the small-field trajectory very closely. However, for the latter case (Fig. 9) the exact trajectory follows the small-field trajectory initially but at the point marked "×" (where $A_+=0.0685$, $A_-=0.0378$, and $\delta=1.25$) the small-field approximation begins to fail, and the full trajectory departs from the small-field trajectory and returns to linear y, which has been stabilized by the high intensity.

The small-field spirals result from the oscillation of both δ and ρ about their critical points. The oscillation of δ occurs at frequency $\approx 2\omega_b$, and either grows or decays exponentially at rate ε depending on whether it is centered about $\delta=0$ (the y axis) or $\delta=\pm\pi$ (the x axis). If the initial seed is near the y axis, with a value $\delta=\delta_i$, the small-field trajectory will circle the y critical point until δ reaches $\approx\pm\pi/2$, at $\tau\approx(\varepsilon)^{-1}\ln(\pi/(2\delta_i))$ at which point it switches to the decreasing spiral centered at $\delta=\pm\pi$. The pitch of each spiral (i.e., the number of revolutions about each critical point) is therefore of order ω_b/ε.

The time that the system remains on the small-field trajectory is determined by conditions (36) and (37), and can be estimated by considering the amplitude growth of small x- or y-polarized fields. For an x-polarized field ($A_+=A_-$, $\delta=\pm\pi$) the amplitude equations [Eq. (27)] reduce to a single equation,

$$\frac{dA_x}{d\tau}=-(1-C\eta_+-\varepsilon)A_x, \tag{44}$$

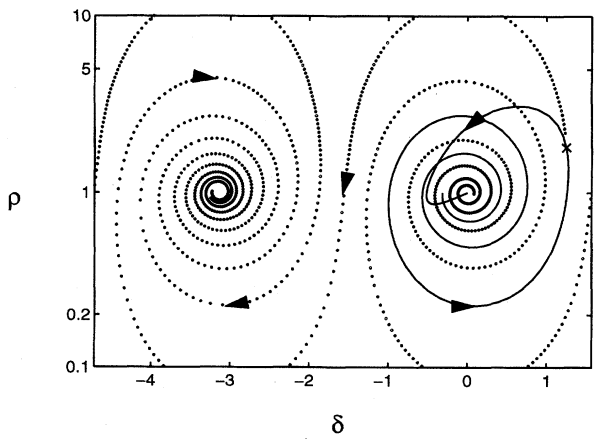

FIG. 9. Example trajectories (dotted lines) for the small field equations, for the same parameters as Fig. 6. The actual trajectory corresponding to Fig. 6 is shown as the solid curve, and at the point "×" where it departs from the small field trajectory, $I_+=4.4\times10^{-3}$ and $I_-=1.4\times10^{-3}$.

which, in the small-field regime where Eqs. (35) and (40) apply, can be written

$$\frac{dA_x}{d\tau}\approx G_xA_x \quad (A_\pm\ll1), \tag{45}$$

where we have defined

$$G_x\equiv\left(\frac{C}{1+\Delta^2}+\varepsilon-1\right). \tag{46}$$

Similarly for a y-polarized field in the small-field limit, the amplitude equations become

$$\frac{dA_y}{d\tau}\approx G_yAy, \tag{47}$$

where

$$G_y\equiv\left(\frac{C}{1+\Delta^2}-\varepsilon-1\right). \tag{48}$$

The net small-field gains G_x and G_y provide the characteristic times (G_x^{-1},G_y^{-1}) over which the fields remain small and remain on the spiral trajectories discussed above. Of course if G_x and $G_y<0$, the losses always outweigh the gains, and no lasing can occur regardless of initial field value.

B. Large-field behavior

When the initial gain is large the field may grow rapidly and independently of the value of δ, to values of $A_\pm$ that are close to their final values. However, the polarization can continue to evolve (e.g., Fig. 4), and the small-field analysis of the preceding section is unable to describe this evolution. In this section we incorporate the effect of the medium into the equation for $d\delta/d\tau$, in order to describe the features of the system behavior that occur once the fields become large, and also to allow us to predict the stability of the output state. Our approach is based on the observation that when the gain becomes saturated ($\tilde{\eta}_+\ll1$), the first term in Eq. (27) becomes a nearly constant damping term allowing the amplitudes to adiabatically follow δ, which is evolving according to Eq. (34). Thus when

$$I_+,I_-\gg\frac{1}{8} \tag{49}$$

so that $\tilde{\eta}_+\ll1$, we set the left-hand side (LHS) of Eq. (27) to zero giving

$$C\frac{\tilde{\eta}_+}{1+\Delta_+^2}=1+\frac{1}{\rho}(\varepsilon\cos\delta-\omega_b\sin\delta) \tag{50}$$

and

$$C\frac{\tilde{\eta}_-}{1+\Delta_-^2}=1+\rho(\varepsilon\cos\delta+\omega_b\sin\delta). \tag{51}$$

For given δ, equations (50), (51), and (28) can be solved (for example, numerically) to find A_+, A_-, $d\phi_+/d\tau$, and $d\phi_-/d\tau$ (and hence $d\delta/d\tau$). This approach is similar to the

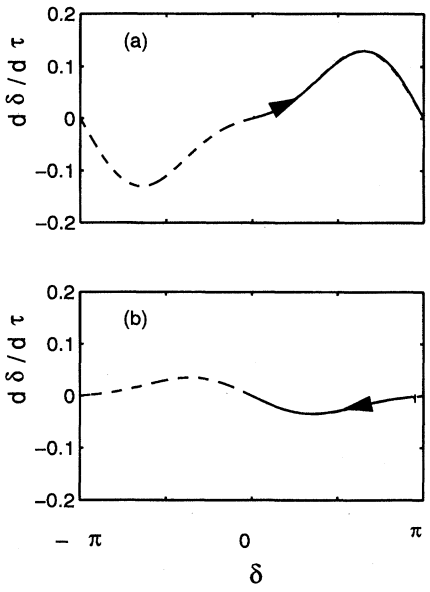

FIG. 10. $d\delta/d\tau$ as a function of δ, for parameters corresponding to (a) Fig. 4 and (b) Fig. 5. The dashed line is the adiabatic approximation and the solid line is the full solution corresponding to each case.

"semi-adiabatic" approximation of van Haeringen and De Lang [11] (also discussed in [12]) but differs in that the total intensity is not assumed to be constant, but is slaved to the value of δ. Using the method just outlined, we have plotted $d\delta/d\tau$ versus δ in Fig. 10(a) for the same parameter values as in Fig. 4, and in Fig. 10(b) for the same parameters as in Fig. 5. For comparison we also plot the $d\delta/d\tau$ versus δ obtained from the full solutions, and it is clear that the corresponding two curves are almost identical. An analytic form for the equation for $d\delta/d\tau$ can be found by using Eqs. (50) and (51) to substitute for $\tilde{\eta}_{\pm}$ in Eq. (34), giving

$$\frac{d\delta}{d\tau}\left(1+\frac{\kappa}{\Gamma}\right)=\omega_b\cos\delta\left(\frac{1}{\rho}-\rho\right)+\varepsilon\sin\delta\left(\frac{1}{\rho}+\rho\right)+\Delta\left[\varepsilon\cos\delta\left(\rho-\frac{1}{\rho}\right)+\omega_b\sin\delta\left(\frac{1}{\rho}+\rho\right)\right]-\frac{\kappa}{\Gamma}\frac{d\phi_+}{d\tau}\left[\frac{1}{\rho}(\varepsilon\cos\delta-\omega_b\sin\delta)\right]+\frac{\kappa}{\Gamma}\frac{d\phi_-}{d\tau}[\rho(\varepsilon\cos\delta+\omega_b\sin\delta)], \tag{52}$$

where we have used the definition of $\Delta_{\pm}$[Eq. (32)]. Noting that $\kappa/\Gamma\ll 1$ and that $\rho\sim 1$, we can ignore the $d\phi_{\pm}/d\tau$ terms on the RHS of the equation, and the κ/Γ correction on the LHS, giving

$$\frac{d\delta}{d\tau}\approx\omega_b\cos\delta\left(\frac{1}{\rho}-\rho\right)+\varepsilon\sin\delta\left(\frac{1}{\rho}+\rho\right)+\Delta\left[\varepsilon\cos\delta\left(\rho-\frac{1}{\rho}\right)+\omega_b\sin\delta\left(\frac{1}{\rho}+\rho\right)\right]. \tag{53}$$

It is possible to eliminate ρ by making what we call the "equal or saturated" approximation (ESA),

$$\tilde{\eta}_+ I_+\approx\tilde{\eta}_- I_-, \tag{54}$$

which will be valid when *either*

$$I_+\approx I_- \tag{55}$$

or

$$I_+ \text{ or } I_-\gg 1/4\beta. \tag{56}$$

Equation (54) can be rewritten as

$$\rho^2\approx\frac{\tilde{\eta}_-(1+\Delta_+^2)}{\tilde{\eta}_+(1+\Delta_-^2)} \tag{57}$$

and then the RHS of the latter equation can be evaluated using Eqs. (50) and (51) to give

$$\rho^2\approx\frac{\rho(\omega_b\sin\delta+\varepsilon\cos\delta)+1}{(-\omega_b\sin\delta+\varepsilon\cos\delta)/\rho+1}, \tag{58}$$

which is equivalent to

$$\rho\approx\omega_b\sin\delta+\sqrt{1+\omega_b^2\sin^2\delta}, \tag{59}$$

where the square root must be positive as A_+ and A_- and hence ρ are non-negative. Notice that Eq. (59) shows that for large fields, if $\delta=0$ or $\pm\pi$, the polarization must be linear ($\rho=1$), while if δ is not a multiple of π the polarization is elliptical ($\rho\neq 1$).

Finally we can use Eq. (59) in Eq. (53) to give

$$\frac{d\delta}{d\tau}=2\varepsilon\sin\delta\sqrt{1+\omega_b^2\sin^2\delta}-\omega_b^2\sin 2\delta+\omega_b\Delta[2\sin\delta\sqrt{1+\omega_b^2\sin^2\delta}+\varepsilon\sin 2\delta], \tag{60}$$

which is an approximate form valid whenever the ESA validity condition holds along the large-field trajectory. We note that a plot of $d\delta/d\tau$ obtained from expression Eq. (60) using the set of parameters in Fig. 4 or Fig. 5 is virtually indistinguishable from the (dashed) numerically evaluated curves shown in Fig. 10. Equation (60) is analogous to the one developed by Van Haeringen [Eq. (94) of Ref. [6]], although his equation does not include the square roots, nor the term involving $\Delta\sin 2\delta$. The main difference [36], however, is that in our equation the only quantity involving the atoms is the cavity-gain center offset Δ, while van Haeringen's equation includes an atomic dispersion function, and a quantity related to the value he assumes for a (constant) total intensity.

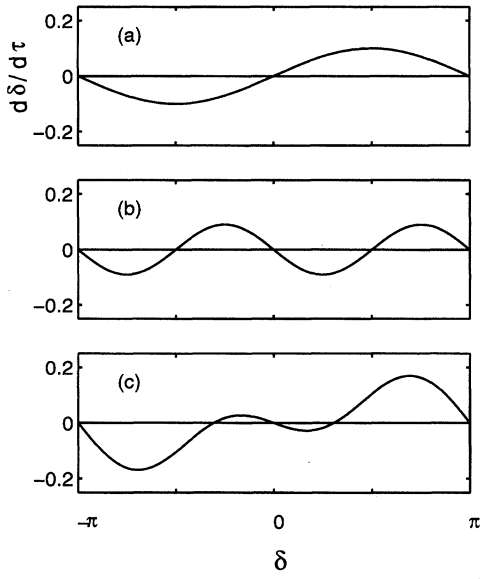

FIG. 11. Plot of the adiabatic equation for $d\delta/d\tau$ [Eq. (60)], showing the effect of absorption and phase anisotropies. (a) $\varepsilon=0.05$, $\omega_b=0$; (b) $\varepsilon=0$, $\omega_b=0.3$, $\Delta=0$; (c) $\varepsilon=0.05$, $\omega_b=0.3$, $\Delta=0$.

C. Role of β

The quantity β contains all the details of the atomic transfer and relaxation processes. When the fields are small, or conversely when the fields are large [see Eq. (49)] and the ESA approximation is satisfied, all such details become irrelevant to the polarization dynamics. The system is sensitive to the value of β only at the intermediate values of the field, but β itself helps determine the boundaries of these regimes [see Eqs. (36) and (56)]. For example, in Fig. 3, where the intensities at $\tau=40$ (at the end of the polarization oscillation) are of order 10^{-11}, the polarization development is determined entirely by the small-field behavior. Since these intensities are so small, β would need to increase by many orders of magnitude before it could effect the solution. In Fig. 4, most of the polarization development occurs once the field intensities have become large, and in this case too there is no sensitivity to β. Of course, if C is decreased so that the fields may never become large enough to allow the large-field analysis to apply, then β can play a role, as discussed at the end of Sec. III. Finally we note that when $\beta \ll 1$, the ESA approximation may fail, even for quite large fields, and the polarization may end up along the axis closest to the initial seed (as remarked in regard to Fig. 6 at the end of Sec. III).

V. SOLUTION FEATURES OF THE LARGE-FIELD EQUATION

A. Overview

Equation (60) is a relatively simple equation that can be used to explain many of the features of the evolution of the laser polarization to its final state. For example, in the most trivial case, where the cavity has no polarization asymmetry ($\varepsilon=0$, $\omega_b=0$), $d\delta/d\tau=0$ as expected, and there is no preferred polarization state. More generally, the curve of $d\delta/d\tau$ versus δ has zero crossings representing steady-state solutions, which are stable if the slope is negative and unstable if the slope is positive.

For the case where the cavity has only absorption asymmetry ($\varepsilon\neq 0$, $\omega_b=0$), then Eq. (60) reduces to $d\delta/d\tau=2\varepsilon \sin\delta$, which is illustrated in Fig. 11(a). It is clear that regardless of the value of Δ, the only stable state is $\delta=\pm\pi$, which corresponds to linear x polarization in agreement with de Lang and Bouwhuis [37]. The y mode is suppressed by the asymmetry in the mirror reflectivity.

When $\omega_b\neq 0$, i.e., the cavity has linear birefringence and thus different resonant frequencies for the x and y modes, second-harmonic terms ($\sin 2\delta$) are introduced into the $d\delta/d\tau$ equation with a sign and strength determined by the relative values of ω_b, Δ, and ε. We begin by considering the case $\varepsilon=\Delta=0$ and $\omega_b\neq 0$, which corresponds to the cavity resonances being symmetrically placed about the atomic resonance and with x and y modes having equal losses. Equation (60) becomes $d\delta/d\tau=-\omega_b^2 \sin 2\delta$, as illustrated in Fig. 11(b), and the stable final state may be either $\delta=0$ or $\pm\pi$, whichever is closest to the value of δ at the outset of the large-field trajectory. If the initial value of δ is randomly chosen, then each polarization mode is equally likely. Figure 11(c) shows the effect of introducing absorption anisotropy in addition to birefringence (i.e., $\varepsilon\neq 0$ and $\omega_b\neq 0$) for the case $\Delta=0$. The relative magnitude of the $\sin 2\delta$ terms is reduced, and the unstable crossing points move inwards to

$$\delta_c=\pm\sin^{-1}\left[\frac{1}{\omega_b}\sqrt{\frac{\omega_b^4-\varepsilon^2}{\omega_b^2+\varepsilon^2}}\right]. \tag{61}$$

When $\omega_b^2>\varepsilon$, δ_c is real, and the phase anisotropy remains strong enough to overcome the absorption disadvantage, thus allowing y to be a stable steady state (as shown). Conversely, if $\varepsilon>\omega_b^2$, then δ_c is not physical and the absorption asymmetry completely determines the output so that only the x polarization is stable. We note that for the case of Fig. 4, where $\varepsilon-\omega_b^2=0.01$, the $d\delta/d\tau$ versus δ curve is flat and almost zero in the region near $\delta=0$ [see Fig. 10(a)], which enhances the metastability of the initial phase. More generally, however, metastability occurs whenever the seed field is near the unstable polarization axis, and the initial gain is large enough to allow the field amplitudes to develop on a much shorter time scale than δ.

In the most general case, where $\Delta\neq 0$ $\varepsilon\neq 0$, and $\omega_b\neq 0$, the difference in medium dispersion between x and y may, if Δ is sufficiently negative, invert the basic $\sin\delta$ shape of the $d\delta/d\tau$ curve. We illustrate the effect of varying Δ in Figs. 12(a)–12(c), where Δ takes the values $0.2, -0.12, -0.3$, respectively. The most general $d\delta/d\tau$ versus δ curve always has zero crossing points at $\delta=0$ and $\pm\pi$, and, in addition, will have unstable crossing points at

$$\delta_d=\pm\sin^{-1}\left[\sqrt{\frac{\omega_b^2(\Delta\varepsilon-\omega_b)^2-(\varepsilon+\Delta\omega_b)^2}{\omega_b^2(\Delta\varepsilon-\omega_b)^2+(\varepsilon+\Delta\omega_b)^2}}\right]. \tag{62}$$

The additional crossing points δ_d will be physical provided

$$\Delta_1\leq\Delta\leq\Delta_2, \tag{63}$$

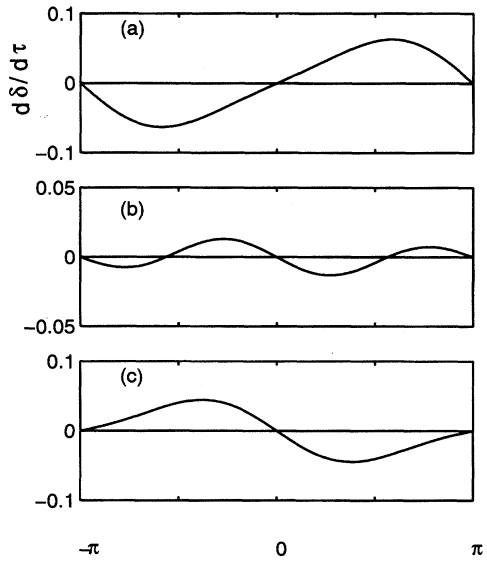

FIG. 12. Plot of the adiabatic equation for $d\delta/d\tau$, showing the effect of varying Δ. (a) $\Delta=0.2$, (b) $\Delta=-0.12$, (c) $\Delta=-0.3$. For each case $\varepsilon=0.01$ and $\omega_b=0.1$.

where

$$\Delta_1 \equiv -\frac{(\omega_b^2+\varepsilon)}{\omega_b(1-\varepsilon)} \tag{64}$$

and

$$\Delta_2 \equiv \frac{(\omega_b^2-\varepsilon)}{\omega_b(1+\varepsilon)}. \tag{65}$$

By evaluating the sign of the derivative $d\delta/d\tau$ at $\delta=0$ and $\pm\pi$, we find that if $\Delta\geq\Delta_2$, only the x polarization is stable [Fig. 12(a)], while if $\Delta\leq\Delta_1$, only the y polarization is stable [Fig. 12(c)]. For the case $\Delta_1<\Delta<\Delta_2$, both x and y polarizations are stable [Fig. 12(b)]. Notice that in the limit of small ω_b, Δ_1 and Δ_2 diverge to $-\infty$, so that only the x stable case lies within the realizable gain region [38]. We can interpret these results physically by noting that for $\omega_b>0$, then when $\Delta<0$ the y mode is closer to the atomic resonance, which may give it sufficient advantage to become the stable lasing state, even though it has higher loss than the x mode.

B. Steady-state behavior

In general (see Sec. III) any steady-state linear polarization must be along either the x or y axis. In addition, we have found, in the large-field approximation, that the *only* stable steady states are linearly polarized along x or y. Consequently, it is worth calculating the steady-state amplitude and frequency for these polarizations. Beginning from Eqs. (27) and (28), setting $A_+=A_-$, $dA_\pm/d\tau=0$, and $d\phi_+/d\tau=d\phi_-/d\tau$ a constant, we can easily eliminate $\tilde{\eta}_\pm$ to obtain the frequency of the x-polarized steady state ($\delta=\pm\pi$),

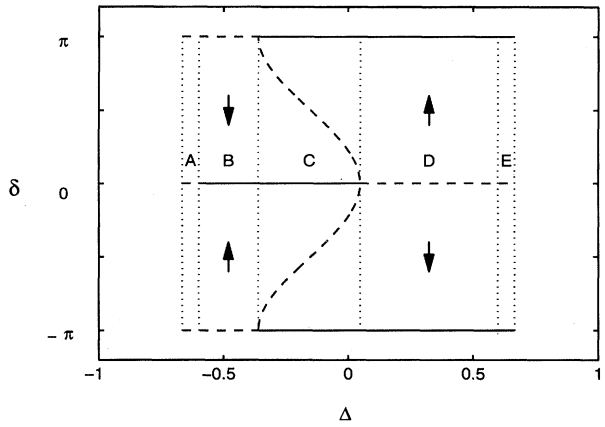

FIG. 13. Stability character of steady state solutions ($d\delta/d\tau=0$) for the case $\omega_b=0.2$, $\varepsilon=0.03$, and $C=1.4$. Stable solutions are shown as solid lines, and unstable solutions as dashed lines. The dotted vertical lines separate regions discussed in the text.

$$\omega_x=\omega+\kappa\frac{d\phi_+}{d\tau}$$

$$=\frac{\kappa(1-\varepsilon)\omega_{u\ell}+\Gamma(\omega-\kappa\omega_b)}{\kappa(1-\varepsilon)+\Gamma}. \tag{66}$$

Equation (66) is recognizable as the standard mode pulling formula for a single mode homogeneously broadened laser [see, e.g., Eq. (5.53) of Ref. [39]], when we recall that $\kappa(1-\varepsilon)$ and $\omega-\kappa\omega_b$ are, respectively, the decay rate and resonant frequency for the x polarization of the empty cavity.

The steady-state value of the electric field, $A_x=\sqrt{2}A_+$, can now be found using the fact that for linear polarization, $\tilde{\eta}_\pm=(1+8I_\pm)^{-1}$, giving

$$A_x^2=\frac{1}{4}\left[\frac{C}{1-\varepsilon}-(1+\Delta_x^2)\right], \tag{67}$$

where $\Delta_x=(\omega_x-\omega_{ul})/\Gamma$. Similarly for the y-polarized steady state,

$$\omega_y=\frac{\kappa(1+\varepsilon)\omega_{u\ell}+\Gamma(\omega+\kappa\omega_b)}{\kappa(1+\varepsilon)+\Gamma} \tag{68}$$

and

$$A_y^2=\frac{1}{4}\left[\frac{C}{1+\varepsilon}-(1+\Delta_y^2)\right]. \tag{69}$$

C. Bistable and oscillatory solutions

The stability information contained in Eq. (60) can be compactly summarized, for given ω_b and ε, by plotting the location of the steady-state solutions on the Δ-δ plane, as shown in Fig. 13. Stable solutions are indicated by solid lines, and unstable solutions by dashed lines. The horizontal lines at $\delta=0$ and $\pm\pi$ are always present, but the curved dashed line in region C, which represents the unstable solution δ_d, moves out of the range of the plot as ω_b becomes

small. Lasing can occur only when the small-field gain G_x [see Eq. (46)] is positive [40], which requires $|\Delta|<\Delta_G$, where

$$\Delta_G \equiv \sqrt{C/(1-\varepsilon)-1} \tag{70}$$

and we indicate these bounds by the outer (dotted) vertical lines at $\pm\Delta_G$. Similarly the dotted vertical lines at $\Delta=\pm\sqrt{C/(1+\varepsilon)-1}$ bound the area where G_y is positive.

We can now see that for systems in regions D and E, the output will always eventually become x polarized, regardless of the initial seed, and that systems in region B will always eventually have y-polarized output. However, in region C, which is bounded by Δ_1 and Δ_2, the final output polarization depends on the value of δ the field achieves by the time the field has become sufficiently large to satisfy our large-field approximation. If the system is to the right of the δ_d curve it will evolve to x polarization, while if it is to the left it will evolve to y polarization. This behavior gives the potential for bistable switching in region C, controlled by scanning Δ (e.g., the cavity length). The switching points are at Δ_1 and Δ_2, and the width of the hysteresis is

$$\Delta_2-\Delta_1=\frac{2(\omega_b^2+\varepsilon^2)}{\omega_b(1-\varepsilon^2)}. \tag{71}$$

We note that in agreement with van Haeringen [6], this region of hysteresis is due to the phase anisotropy (since when $\omega_b\to 0$, Δ_1 and Δ_2 both go to infinity).

Finally we consider the behavior in region A. Initially, only the x component can grow (since $G_y<0$), but when the intensity becomes sufficiently large the system changes to the large-field regime described by Eq. (60), and evolves towards y polarization. Before it becomes pure y-polarized linear, however, the field will be damped (as $G_y<0$) and evolve towards x polarization. An infinite oscillation is set up as seen in Fig. 7, and in some cases may be aperiodic. For this oscillation to occur, there must be both a phase anisotropy, to allow large-field evolution towards y polarization, and an absorption anisotropy, to give a region where $G_y<0<G_x$. Note that for $\varepsilon\ll 1$, the range of Δ values for which $G_y<0<G_x$ is approximately $\varepsilon C/\sqrt{C-1}$.

VI. CONCLUSION

Our model for an anisotropic laser incorporating a full nonperturbative response function for a $J=\frac{1}{2}\leftrightarrow J=\frac{1}{2}$ medium, and a cavity with linear phase and absorption anisotropies, develops further the theory first presented in the classic papers of van Haeringen and Tomlinson and Fork. The parameter regime in which the adiabatic elimination of the atomic medium can be applied is given, and an extensive numerical investigation of the full equations (27) and (28) carried out. The system behavior falls overwhelmingly into three categories, and we have developed simple analytic treatments to characterize and understand this behavior in the small- and large-field regimes. In the case of small fields, we have shown that development of the polarization is determined by the cavity, not the medium. For large fields we have derived an equation for the precession rate of the polarization ellipse which is valid under less restrictive conditions than an analogous equation of van Haeringen and has a simpler form. We have used this equation to analyze the final output polarization states, and conclude that in this regime the only stable output states are linearly polarized along the cavity axes, in agreement with van Haeringen's prediction made on the basis of a third-order perturbative calculation for a $J=\frac{1}{2}\leftrightarrow J=\frac{1}{2}$ medium, e.g., [41]. We have also been able to characterize analytically the regime where the polarization output is bistable, and may flip from one linear polarization to the other as the control parameter Δ is scanned. Additionally, we have identified a regime where the output field undergoes a sustained oscillation, and have given a physical explanation of the mechanisms involved.

In the large-field case, the only atomic parameter to which the solutions are sensitive is the cavity atom detuning Δ. This simple result can be attributed to gain saturation and to the "ESA" approximation Eq. (54), which suppresses the details of the atomic coupling scheme. The latter approximation has a simple interpretation, namely that both the σ^+ and σ^- modes dissipate spontaneous photons at the same rate. If the approximation proved applicable to other atomic transitions, we would expect them to exhibit the same large-field polarization dynamics. Of course, at smaller output field intensities we expect the dynamic behavior to carry the signature of the particular active transition.

APPENDIX A: DENSITY MATRIX EQUATIONS FOR THE ATOMIC MEDIUM

The general form for the density matrix equations for a two level transition with arbitrary j values driven by a laser field has been given in irreducible tensor components by Omont [32]. In this appendix we specialize the results to a $J=\frac{1}{2}\leftrightarrow J=\frac{1}{2}$ transition driven by the superposition of σ^+ and σ^- components represented by Eq. (3). In addition we have incorporated a third level labeled s (of unspecified j value) to act as a reservoir for the lasing transition, providing gain via incoherent population transfer. We shall represent the population of this level by $\rho(s)$, and note that overall population is conserved according to

$$\sqrt{2}\rho_0^0(u)+\sqrt{2}\rho_0^0(l)+\rho(s)=1. \tag{A1}$$

The full density matrix equations are

$$\frac{\partial\rho_0^0(u)}{\partial t}=-\gamma_u\rho_0^0(u)+\frac{\lambda_u}{\sqrt{2}}\rho(s) -2\mathrm{Im}\{iv[\mathscr{E}_-\rho_1^1(lu)+\mathscr{E}_+\rho_{-1}^1(lu)]\}, \tag{A2}$$

$$\frac{\partial\rho_0^0(l)}{\partial t}=-\gamma_l\rho_0^0(l)+\gamma\rho_0^0(u)+\frac{\lambda_l}{\sqrt{2}}\rho(s) +2\mathrm{Im}\{v[\mathscr{E}_-\rho_1^1(lu)+\mathscr{E}_+\rho_{-1}^1(lu)]\}, \tag{A3}$$

$$\frac{\partial\rho(s)}{\partial t}=-(\lambda_u+\lambda_l)\rho(s)+\sqrt{2}(\gamma_u-\gamma)\rho_0^0(u)+\sqrt{2}\gamma_l\rho_0^0(l), \tag{A4}$$

$$\frac{\partial\rho_0^1(l)}{\partial t}=-\Gamma_1(l)\rho_0^1(l)-\frac{\gamma}{3}\rho_0^1(u)+2\mathrm{Im}\{v[\mathscr{E}_-\rho_1^1(lu)-\mathscr{E}_+\rho_{-1}^1(lu)]\},\quad\text{(A5)}$$

$$\frac{\partial\rho_0^1(u)}{\partial t}=-\Gamma_1(u)\rho_0^1(u)+2\mathrm{Im}\{v[\mathscr{E}_-\rho_1^1(lu)-\mathscr{E}_+\rho_{-1}^1(lu)]\},\quad\text{(A6)}$$

$$\frac{\partial\rho_1^1(lu)}{\partial t}=-(\Gamma-i\omega_{ul})\rho_1^1(lu)+i(v\mathscr{E}_-)^*[\rho_0^0(u)-\rho_0^0(l)-\rho_0^1(u)-\rho_0^1(l)],\quad\text{(A7)}$$

$$\frac{\partial\rho_{-1}^1(lu)}{\partial t}=-(\Gamma-i\omega_{ul})\rho_{-1}^1(lu)+i(v\mathscr{E}_+)^*[\rho_0^0(u)-\rho_0^0(l)+\rho_0^1(u)+\rho_0^1(l)].\quad\text{(A8)}$$

We note that the density matrix components are real, apart from $\rho_1^1(lu)$ and $\rho_{-1}^1(lu)$, and that

$$v=\sqrt{\frac{\Gamma\gamma}{\mu}}e^{-i\omega t}.\quad\text{(A9)}$$

The orientation decay rate $\Gamma_1(u)$ of the upper level is related to the collision rate κ_u by

$$\Gamma_1(u)=2\kappa_u+\gamma_u,\quad\text{(A10)}$$

and a similar equation holds for $\Gamma_1(l)$.

APPENDIX B: ANISOTROPIC CAVITY BOUNDARY CONDITIONS

1. Scalar field

The boundary condition for a *scalar* field propagating around an (isotropic) ring cavity is [34]

$$E(z=0,t)=re^{-i\psi}E(L,t-(\Lambda-L)/c),\quad\text{(B1)}$$

where $r\exp(-i\psi)$, with r and ψ real, is the reflectivity of the output mirror.

Converting (B1) into an equation for the slowly varying field component $\mathscr{E}$ defined by

$$E(z,t)=\mathscr{E}(z,t)e^{i(Kz-\Omega t)}\quad\text{(B2)}$$

gives

$$\mathscr{E}(z=0,t)=r\mathscr{E}(L,t-(\Lambda-L)/c)e^{i(KL+\Omega\Lambda-L/c-\psi)},\quad\text{(B3)}$$

which reduces to

$$\mathscr{E}(z=0,t)=r\mathscr{E}(L,t-(\Lambda-L)/c),\quad\text{(B4)}$$

when we note that $K=\Omega/c$ and *assume* that $K\Lambda-\psi=2\pi M$ (M is an integer). $K\Lambda-\psi=2\pi M$ is exactly the condition for a wave to travel once around the cavity without a net phase shift if there is no medium present. Thus we are assuming that Ω is a resonant frequency of the empty cavity.

2. Vector field

In the present work we wish to incorporate a (two-dimensional) vector field with a cavity that has different reflectivities and different resonant frequencies for two perpendicular linear polarizations, i.e., we require

$$\mathbf{E}(z,t)=[\hat{\mathbf{e}}_xE_{\mathrm{sat}}\bar{\mathscr{E}}_x(z,t)e^{i(k_xz-\omega_xt)}+\hat{\mathbf{e}}_yE_{\mathrm{sat}}\bar{\mathscr{E}}_y(z,t)e^{i(k_yz-\omega_yt)}]+\text{c.c.},\quad\text{(B5)}$$

where [42]

$$\bar{\mathscr{E}}_x(0,t)=r_x\bar{\mathscr{E}}_x(L,t-(\Lambda-L)/c)\quad\text{(B6)}$$

and

$$\bar{\mathscr{E}}_y(0,t)=r_y\bar{\mathscr{E}}_y(L,t-(\Lambda-L)/c)\quad\text{(B7)}$$

with r_x and r_y real, $0<r_y,r_x<1$, and $\omega_x\neq\omega_y$. Comparing Eq. (B5) with Eq. (1), i.e., factoring out the same rapidly varying frequency from the two components, we have

$$\mathbf{E}(z,t)=\mathscr{E}(z,t)E_{\mathrm{sat}}e^{i(kz-\omega t)}+\text{c.c.},\quad\text{(B8)}$$

where

$$\mathscr{E}=\mathscr{E}_x\hat{\mathbf{e}}_x+\mathscr{E}_y\hat{\mathbf{e}}_y,\quad\text{(B9)}$$

$$\mathscr{E}_x=\bar{\mathscr{E}}_xe^{i(\omega_x-\omega)(z/c-t)},\quad\text{(B10)}$$

$$\mathscr{E}_y=\bar{\mathscr{E}}_y{}^{i(\omega_y-\omega)(z/c-t)},\quad\text{(B11)}$$

and hence Eqs. (B6) and (B7) become

$$\mathscr{E}_x(0,t)=r_xe^{-i(\omega_x-\omega)(\Lambda/c)}\mathscr{E}_x\left(L,t-\frac{\Lambda-L}{c}\right)\quad\text{(B12)}$$

and

$$\mathscr{E}_y(0,t)=r_ye^{-i(\omega_y-\omega)(\Lambda/c)}\mathscr{E}_y\left(L,t-\frac{\Lambda-L}{c}\right).\quad\text{(B13)}$$

ω is still arbitrary (within the constraints of the SVEA) and so for symmetry we *choose*

$$\omega=\frac{\omega_y+\omega_x}{2},\quad\text{(B14)}$$

and combine Eqs. (B12) and (B13) to give

$$\begin{pmatrix}\mathscr{E}_x(0,t)\\ \mathscr{E}_y(0,t)\end{pmatrix}=R_{xy}\begin{pmatrix}\mathscr{E}_x\left(L,t-\frac{\Lambda-L}{c}\right)\\ \mathscr{E}_y\left(L,t-\frac{\Lambda-L}{c}\right)\end{pmatrix},\quad\text{(B15)}$$

where

$$R_{xy}=\begin{pmatrix}r_xe^{i\theta}&0\\0&r_ye^{-i\theta}\end{pmatrix}\quad\text{(B16)}$$

and we have set

$$\theta=\frac{\Lambda}{c}\frac{\omega_y-\omega_x}{2}. \tag{B17}$$

Thus the frequency of the rapidly oscillating part of the electric field, ω, lies midway between the two empty cavity resonances. Representing Eq. (B15) in terms of $\mathscr{E}_\pm$ allows us to obtain the boundary condition in terms of circular components, namely

$$\begin{pmatrix}\mathscr{E}_+(0,t)\\ \mathscr{E}_-(0,t)\end{pmatrix}=R_{\rm circ}\begin{pmatrix}\mathscr{E}_+\left(L,t-\dfrac{\Lambda-L}{c}\right)\\ \mathscr{E}_-\left(L,t-\dfrac{\Lambda-L}{c}\right)\end{pmatrix}, \tag{B18}$$

where

$$R_{\rm circ}=\frac{1}{2}\begin{pmatrix}r_xe^{i\theta}+r_ye^{-i\theta}, & r_ye^{-i\theta}-r_xe^{i\theta}\\ r_ye^{-i\theta}-r_xe^{i\theta}, & r_xe^{i\theta}+r_ye^{-i\theta}\end{pmatrix}. \tag{B19}$$

[1] L. Casperson, IEEE J. Quantum Electron. **QE-14**, 756 (1978).
[2] J. Opt. Soc. Am. B **2** (1985), special issue on Instabilities in Active Optical Media, edited by N. B. Abraham, L. A. Lugiato, and L. M. Narducci.
[3] J. Opt. Soc. Am. B **7** (1990), special issue on Transverse Effects in Non-linear Optical Systems, edited by N. B. Abraham and W. J. Firth.
[4] H. Statz, R. Paananen, and G. F. Koster, J. Appl. Phys. **33**, 2319 (1962).
[5] W. Culshaw and J. Kannelaud, Phys. Rev. **136**, 1209 (1964).
[6] W. van Haeringen, Phys. Rev. **158**, 256 (1967).
[7] M. Sargent, W. E. Lamb, and R. L. Fork, Phys. Rev. **164**, 436 (1967).
[8] W. J. Tomlinson and R. L. Fork, Phys. Rev. **164**, 466 (1967).
[9] L. Gil, Phys. Rev. Lett. **70**, 162 (1993).
[10] R. Corbalan *et al.*, Phys. Rev. A **48**, 1483 (1993).
[11] W. van Haeringen and H. de Lang, Phys. Rev. **180**, 624 (1969).
[12] W. J. Tomlinson and R. L. Fork, Phys. Rev. **180**, 628 (1969).
[13] A. L. Floch, R. L. Naour, and G. Stephan, Opt. Commun. **20**, 42 (1977).
[14] A. L. Floch, G. Ropars, J. M. Lenormand, and R. L. Naour, Phys. Rev. Lett. **52**, 918 (1984).
[15] P. Glorieux and A. L. Floch, Opt. Commun. **79**, 229 (1990).
[16] D. Jacob, J. C. Cotterverte, A. L. Floch, and F. Bretenaker, J. Phys. France **4**, 367 (1994).
[17] A. L. Floch, Ann. Phys. **15**, 121 (1990).
[18] J. C. Cotterverte, F. Bretenaker, and A. L. Floch, Opt. Lett. **16**, 572 (1991).
[19] S. Grossmann and D. Yao, Z. Phys. B **80**, 439 (1990).
[20] M. W. Hamilton, R. J. Ballagh, and W. J. Sandle, Z. Phys. B **49**, 263 (1982).
[21] R. J. Ballagh and V. Jain, Philos. Trans. R. Soc. London Ser. A **313**, 445 (1984).
[22] C. Parigger, P. Hannaford, and W. J. Sandle, Phys. Rev. A **34**, 2058 (1986).
[23] A. W. McCord and R. J. Ballagh, J. Opt. Soc. Am. B **7**, 73 (1990).
[24] D. E. McClelland, H. A. Bachor, and J. C. Wang, Opt. Commun. **84**, 184 (1991).
[25] A. C. Wilson *et al.*, Opt. Commun. **88**, 67 (1992).
[26] R. J. Ballagh and A. W. McCord, Int. J. Nonlinear Opt. Phys. **1**, 393 (1992).
[27] A. Eschmann and C. W. Gardiner, Phys. Rev. A **49**, 2907 (1994).
[28] L. A. Lugiato, P. Mandel, and L. Narducci, Phys. Rev. A **29**, 1438 (1984).
[29] W. J. Sandle, M. W. Hamilton, and R. J. Ballagh, in *Optical Bistability 2*, edited by C. M. Bowden, H. M. Gibbs, and S. L. McCall (Plenum, New York, 1984).
[30] A. Corney, *Atomic and Laser Spectroscopy* (Oxford University Press, Oxford, 1977).
[31] Positive rotation of the field when viewed looking down the z axis to the origin.
[32] A. Omont, Prog. Quantum Electron. **5**, 69 (1977).
[33] L. A. Lugiato, Opt. Commun. **33**, 108 (1980).
[34] L. M. Narducci, in *Laser Physics and Laser Instabilities*, edited by L. M. Narducci and N. B. Abraham (World Scientific, Singapore, 1988).
[35] Equations (42) and (43) are meaningful only when both σ^+ and σ^- are present.
[36] In van Haeringen's Eq. (94) we may put $\theta_1=\theta_2=0$ (since our cavity axes are 90° apart), $H_z=0$ (zero magnetic field), and identify a as $2\kappa\varepsilon$ and ϕ_0 as $2\kappa\omega_b$.
[37] H. de Lang and G. Bouwhuis, Phys. Lett. **20**, 383 (1966).
[38] In this discussion we have, for convenience, chosen both ω_b and ε positive, and Eqs. (62)–(65) apply for $\omega_b>0$. The form of Δ_1 and Δ_2 for $\omega_b<0$ is very similar.
[39] K. Shimoda, *Introduction to Laser Physics* (Springer-Verlag, Berlin, 1984).
[40] For convenience we have assumed ε is positive, but if negative, the roles of G_x and G_y are reversed.
[41] D. Polder and W. van Haeringen, Phys. Lett. **19**, 380 (1965).
[42] We assume that, although $\mathscr{E}_x$ and $\mathscr{E}_y$ undergo a relative phase shift at the output mirror, they have the same transit time $(\Lambda-L)/c$ between exiting the medium and reentering it.